J Intell Robot Syst (2010) 57:281–295
DOI 10.1007/s10846-009-9358-2

Exploring the Effect of Obscurants on Safe Landing Zone Identification

Keith W. Sevcik · Noah Kuntz · Paul Y. Oh

Received: 1 February 2009 / Accepted: 1 August 2009 / Published online: 28 August 2009

Abstract Manned rotorcraft are often employed in harsh environments and difficult terrain that are inaccessible to other craft. Conversely, robotic rotorcraft are operated in controlled settings, often at safe, high altitudes. Missions such as cargo delivery, medevac and fire fighting are unachievable because of unpredictable adverse environmental conditions. To enable UAVs to perform these missions, the effects of obscurants on UAV sensor suites and algorithms must be clearly understood. This paper explores the use of a laser range finder to accomplish landing zone identification in unknown, unstructured environments. The ability to detect a landing zone in environments obscured by smoke is investigated. This is accomplished using a design methodology of testing and evaluating in a controlled environment followed by verification and validation in the field. This methodology establishes a concrete understanding of the sensor performance, thereby removing ambiguities in field tests.

Keywords Evaluating guidance algorithms · Verifying performance · Navigation and control

1 Introduction

Helicopters and other manned rotorcraft often perform missions that can not be accomplished by other craft. Their ability to fly and hover allows helicopters to access

K. W. Sevcik · N. Kuntz · P. Y. Oh (✉)
Department of Mechanical Engineering and Mechanics, Drexel University,
3141 Chestnut Street, Philadelphia, PA, USA
e-mail: paul@coe.drexel.edu

K. W. Sevcik
e-mail: kws23@drexel.edu

N. Kuntz
e-mail: nk752@drexel.edu

remote terrain amongst obstacles like buildings, poles and trees. Pilots are able to perform missions such as cargo delivery, search and rescue, and fire fighting even when faced with thick smoke and brown-out conditions.

Conversely, robotic rotorcraft are often confined to well structured, safe environments. Missions such as surveillance are performed at high altitudes, safe from the threat of obstacles on the ground. In other tasks such as building inspection, the rotorcraft is often controlled by a pilot who has a constant line of sight to the aircraft. When these tasks are made autonomous, the ambient conditions are often chosen to be idyllic without adverse weather conditions. To enable UAVs to perform the missions carried out by manned helicopters, the effects of obscurants on UAV sensor suites and algorithms must be clearly understood.

In evaluating this problem, a baseline capability must be identified for testing. Landing zone identification is an essential component to many rotorcraft missions. The problem extends to tasks such as cargo delivery, medevac and search and rescue among others. Landing zone identification is a thoroughly researched problem, and many well developed solutions already exist. Furthermore, the capabilities necessary for landing zone detection are extensible to other core capabilities, such as obstacle avoidance and mapping.

Landing zone identification requires a sensor suite capable of mapping the ground beneath the helicopter. Selecting a sensor suite for this task is complicated by the nature of the environments in which these robots operate. Areas of interest such as urban landscapes are cluttered with obstacles. Large structures like buildings can be easily detected by many different types of sensors. Small obstacles like wires and sparse obstacles such as trees and bushes can be more difficult to detect. These pose great risk to rotorcraft because the exposed rotor is easily damaged, even by small objects. This potential hazard demands a sensor suite capable of resolving small obstacles at far ranges.

Furthermore, the robot may be subject to adverse ambient conditions. Particles from debris or smoke from fires can obscure the field of view of a sensor suite. When a rotorcraft is landing, dust is often scattered, at times creating a brown out effect. To ensure that performance is robust and reliable, these effects must be quantified when addressing the issue of landing zone identification.

As a Future Combat Systems: One Team member, we have gained extensive experience designing sensor suites for robots flying in near-Earth environments. The Future Combat Systems (FCS) Class II program focused on building a UAV to fly missions in near-earth environments such as urban terrain and forests. This project identified a few fundamental requirements for sensor suites.

The sensor must detect a wide range of obstacles. In urban terrain, object size and composition can vary drastically, from buildings to telephone poles to thin wires and clothes lines. In particular, sparse objects such as trees and bushes are troublesome to detect.

The UAV will also encounter a variety of adverse environmental conditions, such as the scenario depicted in Fig. 1. Smoke from fires or dust from down-wash can hinder the performance of the UAVs sensor suite. Other environmental factors such as rain, fog, and varied lighting can further degrade performance. The selected sensor must adequately address these issues.

Our experiences in sensor suite design revealed that scanning laser range finders are the best suited sensor to meet these criteria. Preliminary experiments against the

Fig. 1 The SR100 robotic rotorcraft hovers over an unsafe landing site. A laser range finder mounted to the bottom of the craft is tested for its performance in smoke

criteria stated above showed them to out perform common sensors such as sonar, computer vision and optic flow.

The biggest attraction of these sensors is their high fidelity and wide field of view. Their range is comparable if not better than many traditional sensors. Laser range finders are also able to clearly detect many different objects including sparse objects such as trees and bushes. Additionally, they are robust to varied lighting, encountering difficulties only in extreme conditions such as direct sunlight measuring over 10,000 lux.

The major drawback to laser range finders is their sensitivity to obscurants present in the air. Rain can cause reflections that appear to be thin obstacles. Additionally, particulate matter such as fog, smoke and dust attenuate the laser beam and cause back-scatter, making some obstacles undetectable. This detriment can hinder the operational capabilities of the UAV.

Extensive work has been done to model the effect of obscurants. A model for the effect of different kinds of smoke and various other obscurants is presented in [1]. Brinkworth [2] defines general equations for determining attenuation and back-scatter from a light source. Such models can be used to correct for obscurants in laser range measurements.

Other researchers have directly measured the effects of fog and smoke on lasers. Arshinov et al. [3] conclude that back-scatter from lasers is more affected by the amount of smoke and fog than the wavelength of the laser. Even though these effects are well documented and measured, there has been relatively little work towards applying the results to the problem of building terrain maps and identifying safe landing zones.

Laser range finders have proven their capability for mapping cluttered terrain. In [4] a laser range finder mounted to a rotorcraft is used to map buildings, bushes and trees. Previous work has also demonstrated the ability to navigate rotorcraft based on these maps. A LADAR sensor was used to map urban terrain in [5]. Obstacles as small as 6mm diameter wires were successfully detected. This map was then

used to autonomously guide the craft through the environment. These experiments noticed effects from dust, however the research did not extend to characterizing and correcting for these effects. Also, these experiments did not explore using the LADAR generated maps to land the vehicle.

Landing rotorcraft autonomously has been accomplished before. Saripalli et al. [6] successfully demonstrated landing a rotorcraft utilizing GPS information and a vision based approach. The same authors demonstrated the ability to land a rotorcraft on a moving target in [7] using similar techniques. Both of these results rely on predetermined GPS locations where well marked fiducials are placed on the ground. Such well structured scenes would not necessarily be available in a perch-and-stare or cargo delivery missions.

Algorithms for safe landing zone identification have also been presented and tested. Both [8] and [9] present machine vision based approaches for identifying safe landing zones. While the fundamental approach can be applied to any terrain map, the specific algorithms assume images, which could be degraded by obscurants. In [10], an algorithm is presented for identifying safe landing zones using a laser range finder. This body of research shows that the individual components exist to detect landing zones while accounting for adverse conditions.

This paper examines the effects of obscurants on identifying safe landing zones. A method for determining a safe landing zone using a LADAR sensor on board a robotic rotorcraft is presented. This method is comprised of a step in which the terrain map is reconstructed from laser and position data, followed by a step in which the safest landing zone in the terrain map is identified. A SICK LMS200 laser range finder was tested and evaluated for varying densities of smoke inside a UAV testing facility. The sensor model with and without obscurants was determined from these experiments. Verification and validation was performed on board an SR100 robotic helicopter. Results from these experiments are presented.

Section 2 describes the approach used to generate terrain maps and identify landing zones. Section 3 describes the testing and evaluation of the SICK laser utilizing SISTR, a Systems Integrated Sensor Test Rig. The robotic platform used for verification and validation is described in Section 4. Preliminary experimental results are given in Section 5. Finally, conclusions and future work are discussed in Section 6.

2 Algorithms

To detect a safe area to land, the robot must first generate a map of its environment. This terrain map is generated using the laser scans and pose measurements of the aircraft. Vibrations from the helicopter and inherent noise/drift in the sensors can seriously degrade the quality of the terrain map. To recover a usable map of the terrain, a mapping algorithm must be applied that considers noise in both measurements. The resulting terrain map is often comprised of large flat areas with both large and small obstacles. The landing zone algorithm must find flat, obstacle free terrain with a large enough area to fit the rotorcraft. The following sections describe the algorithms utilized to accomplish these steps.

2.1 Mapping

To generate a terrain map, laser scans must be fused with relatively noisy pose measurements. This is accomplished using an implementation of the process presented in [4]. The fundamental concepts and their application are presented here in brief.

This algorithm produces a 3D map of the environment given noisy pose and terrain measurements. To find the corrected pose, a probabilistic model is constructed. This model is comprised of: the probability of the pose measurement, the probability of differential pose measurements, and the probability of consecutive scan alignment.

The probability of pose measurement is modeled as the probability of measuring the pose given the corrected pose. The system is taken to be 6 degrees of freedom, namely the 3 Cartesian coordinates and rotations about those axes. Their measurement at the current time step is the vector y_t, while the algorithm solves for the corrected pose x_t. Given the measurement covariance A, the probability of y_t given x_t as presented in [4] is then:

$$p(y_t|x_t) \propto \exp\left(-\frac{1}{2}(y_t - x_t)^T A^{-1}(y_t - x_t)\right) \tag{1}$$

The method also utilizes a differential model. Typically, the sensors onboard an aircraft measure rotational and translational rates. The pose is recovered through integration, making it susceptible to drift. The differential model is less affected by this error. Given D, the covariance of differential measurements, the differential model as derived in [4] is:

$$p(\Delta y_t|\Delta x_t) \propto \exp\left(-\frac{1}{2}(\Delta y_t - \Delta x_t)^T D^{-1}(\Delta y_t - \Delta x_t)\right) \tag{2}$$

where $\Delta y_t = y_t - y_{t-1}$ and $\Delta x_t = x_t - x_{t-1}$. As differential measurements are more accurate than absolute measurements, the covariance matrix D should represent a Gaussian with smaller standard deviation than A.

The final portion of the model is a representation of the likelihood of a scan. Rather than representing individual features as states as in traditional SLAM, the implementation in [4] models the consistency between consecutive scans as:

$$p(z_t|x_t, x_{t-1}, z_{t-1}) \propto \prod_i \exp\left(-\frac{1}{2}\min\left[\alpha, \min_j (z_t^i - f(z_{t-1}^j, x_{t-1}, x_t))^T B^{-1}(z_t^i - f(z_{t-1}^j, x_{t-1}, x_t))\right]\right) \tag{3}$$

The goal of this model is to align points from the current scan with points from the previous scan. A point in the current scan z_t^i is compared to all points from the previous scan z_{t-1}. The function f maps a point from the previous scan z_{t-1}^j into the local coordinate system of the current scan z_t. The inner minimization identifies a point from the previous scan that is closest to the point from the current scan. The outer minimization thresholds this alignment to allow for local inconsistencies such as those from sparse objects. The matrix B is the measurement covariance.

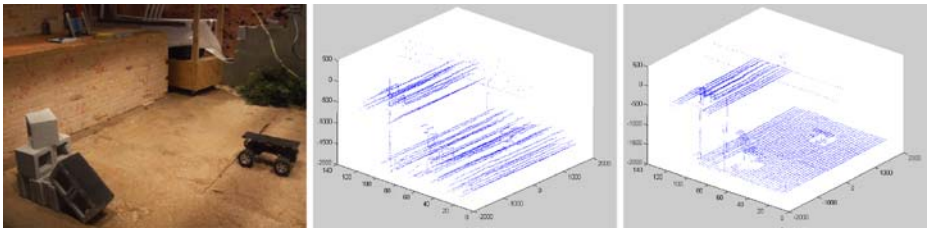

Fig. 2 The sensor was scanned through a mock urban environment (*left*). Gaussian noise was added to the pose measurement to simulate data gathered from a helicopter (*center*). The terrain map was then reconstructed using the algorithm described (*right*)

Equations 1, 2 and 3 can be combined to form the probabilistic model for the entire problem [4]:

$$p(y_t|x_t)p(\Delta y_t|\Delta x_t)p(z_t|x_t, x_{t-1}, z_{t-1}) \tag{4}$$

The map and pose are recovered by finding the pose that maximizes this likelihood, or by minimizing the negative log likelihood given by [4]:

$$\begin{aligned} const + \frac{1}{2}((y_t - x_t)^T A^{-1}(y_t - x_t) + (\Delta y_t - \Delta x_t)^T D^{-1}(\Delta y_t - \Delta x_t) \\ + \sum_i \min[\alpha, \min_j (z_t^i - f(z_{t-1}^j, x_{t-1}, x_t))^T B^{-1}(z_t^i - f(z_{t-1}^j, x_{t-1}, x_t))]) \end{aligned} \tag{5}$$

This minimization is found by first minimizing to associate points from the current scan with those from the previous scan, and then performing hill-climbing to determine the pose that minimizes the negative log likelihood. These steps can be iterated until the negative log likelihood falls within a threshold.

This algorithm was tested on a data set gathered inside a mock urban environment. A test was conducted in which the laser scanner was suspended approximately $2m$ above the ground and oriented to face the ground. The sensor was then traversed through the environment using a robotic gantry. The position of the laser was measured from the gantry's encoders. These conditions were well controlled and the measurements were very accurate, unlike those of a rotorcraft. To simulate noisy pose measurements from a helicopter, Gaussian noise was added to the position data. The results are shown in Fig. 2.

As can be seen, the algorithm successfully recovers the terrain map in the form of a point cloud. The algorithm is able to line up scans and correct the small deviations between measurements. At the same time, it ignores the large deviations, recognizing the discontinuity is actually the ledge of a building. Obstacles such as the truck and cinder blocks are clearly recovered. Even small features are resolved, such as the ridge in the floor from overlapping floor mats. This terrain map can now be used to detect a safe landing zone.

2.2 Safe Landing Zone ID

The algorithm presented in [10] provides robust detection of a safe landing zone based on the input of a point cloud terrain map from a LADAR scanner (Fig. 3).

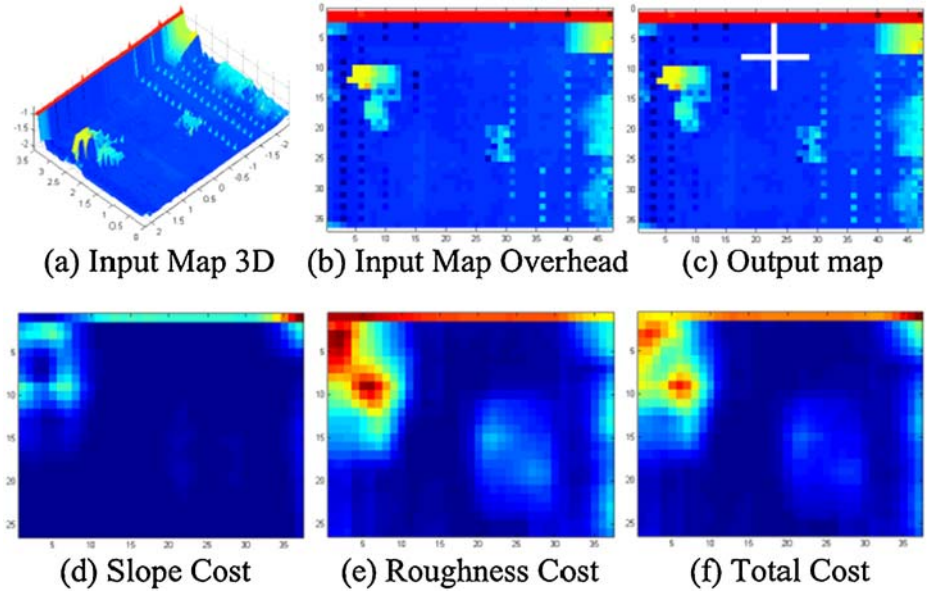

Fig. 3 A terrain image is generated from the LADAR point cloud map. A cost map is then calculated based on the slope of the terrain and the local roughness. The safe landing zone, marked with a cross, is determined as the lowest cost area that fits the helicopter rotor diameter. **a** Input map 3D. **b** Input map overhead. **c** Output map. **d** Slope cost. **e** Roughness cost. **f** Total cost

This algorithm parameterizes a safe landing zone based on the slope of the landing area and the surface roughness. Costs are assigned to the terrain based on these factors, and the lowest cost area which fits the helicopter rotor is selected. Our implementation of this algorithm is described below.

Because of the design of the laser scanner, the resulting point cloud is an irregularly spaced sampling of the scanned surface. A safe landing zone algorithm that uses this data would be intrinsically complicated and resource intensive. To simplify the implementation, the point cloud map is first converted into an image containing regularly spaced pixels. First the size of the grid cells must be determined. The width of each grid cell, C_w, is based on the angular resolution of the scanner θ and the average range to the surface R. The total width of the grid, G_w, is based on the field of view of the scanner f and the average range to the surface. The width of each cell, the total width of the grid and the total number of cells n is then:

$$C_w = 2R\tan(\theta/2) \tag{6}$$

$$G_w = 2R\tan(f/2) \tag{7}$$

$$n = G_w/C_w \tag{8}$$

The cell height was taken to be the same as the cell width. The total grid height G_h is determined from the distance traversed in the direction perpendicular to the scan

plane. This formulation ensures there will not be multiple points per grid cell. After determining the cell and grid sizing, the (x, y) coordinates of data points in the point cloud must be transformed to (r, c) coordinates in the grid. This is accomplished using the relation [10]:

$$(r, c) = (y/C_w + G_h/2, x/C_w + G_w/2) \tag{9}$$

The value of each grid cell is based on the z-coordinate of the points. Interpolation is used to define cells that fall in-between points. The resulting 2D array is analogous to a grayscale image who's pixel values correspond to the height of the terrain. This image is the raw elevation map.

To perform safe landing zone identification, the elevation map is separated into a surface roughness map and a landing incidence angle map. Both these maps require that an underlying smoothed surface first be determined. This surface is formed by fitting square planes the size of the helicopter rotor diameter to the terrain map. Planes are represented as [10]:

$$\mathbf{n} \cdot \mathbf{x} + d = 0 \tag{10}$$

Where the fitted plane at cell $\mathbf{x} = (x, y, z)$ is described by $(\mathbf{n}, d) = (n_x, n_y, n_z, d)$. These planes are fitted with an increment of 1/8 the rotor diameter between planes. The resolution for the position of the chosen landing zone is therefore 1/8 that of the helicopter rotor diameter. Smaller increments could be chosen to make this position more precise. This would come at the cost of processing speed. Due to error in the accuracy of the helicopter's pose measurement, the chosen resolution is believed to be sufficiently accurate.

The landing incidence angle α is calculated using the fitted planes and the geodetic normal of the surface n_g [10]:

$$\alpha = \cos^{-1}(\mathbf{n} \cdot n_g / \|\mathbf{n}\| \|n_g\|) \tag{11}$$

These fitted planes are also used to calculate the smoothed elevation map, where the smooth elevation z_s is given by [10]:

$$z_s = -(n_x x + n_y + d)/n_z \tag{12}$$

Once the smoothed surface is generated, the roughness map can be determined. The roughness map $R(r, c)$ is calculated by subtracting the smoothed elevation map $Z_s(r, c)$ from the original elevation map $Z(r, c)$ and taking the mean [10]:

$$R(r, c) = |Z(r, c) - Z_s(r, c)| \tag{13}$$

A safe landing zone is chosen from a cost map. A cost is calculated for a region based on a weighted sum of the roughness and the slope. The weightings are chosen such that areas with a high roughness (and therefore obstacle rich) are avoided first. The remaining areas are then avoided if the landing incidence angle is too high. These weights are chosen based on the requirements of the platform.

By applying these algorithms successively, the rotorcraft can generate a map and locate a place to land. However, it is still unclear how this process will be effected by environmental conditions. A robust and reliable solution must consider the effect of obscurants. The performance of these algorithms is directly dependent on the ability of the sensor to measure the environment. To gain insight into how the algorithms

will be effected, the sensor was tested and evaluated to characterize its performance in smoke.

3 Obscurant Testing and Evaluation

The path for evaluating UAV algorithms developed in the lab is to perform flight tests. While flight tests are necessary to ensure the validity of the algorithm, unpredictable conditions can often lead to inconclusive results. We choose to gain a full understanding of the performance of our sensors and algorithms by introducing acclimment conditions in a controlled environment. This process of testing and evaluation gives a clear understanding of how the sensor and algorithms operate. The flight test is then a verification of the results measured in the lab.

3.1 SISTR

Assessing the performance of the sensor requires a testing facility capable of repeatably and controllably simulating realistic environments. SISTR, shown in Fig. 4, is a National Science Foundation funded UAV testing facility that provides this capability. SISTR measures 19 ft. x 18 ft. x 20 ft. enclosing a mock urban environment constructed at full scale with actual materials such as plywood, brick and cinder blocks. The environment can be augmented and reconfigured with other features such as poles, wires and trees to test robustness to varying obstacles.

As described in [11], the facility is surrounded by a six degree-of-freedom computer controlled gantry. Using the math model that describes the flight dynamics of an aircraft, the gantry can be programmed to mimic the flight of a vehicle. Table 1 displays the maximum and minimum velocities achievable by the gantry. While these velocities do not represent the full range of velocities achievable by UAVs, they

Fig. 4 Systems Integrated Sensor Test Rig (SISTR). SISTR provides a stage for testing and evaluation of hardware in simulated urban environments and disaster scenarios. Effects such as varied lighting, rain, fog and smoke can be introduced in a controlled and repeatable fashion

Table 1 SISTR velocities

Axis	Velocity range
X	0.012–0.61m/s
Y	0.019–0.61m/s
Z	0.021–0.61m/s

do encompass a portion of the operating range for rotorcraft. The position in all translational axes of the gantry can be controlled to within $\pm 0.5cm$.

Sensor packages can be mounted on SISTR and virtually flown through an environment. Sensor data is collected in real time by the same control algorithms and software that would be used in flight. The control commands are fed into a mathematical model of the aircraft, which generates aircraft positions. These positions are then played back on SISTR.

SISTR is also equipped with testing apparatus to simulate different environmental conditions. There are some permanent fixtures. Stage lights placed near the top of the facility can be individually controlled to create varied lighting scenarios. Light-blocking curtains can be used to create night time conditions. Other environmental fixtures can be added as needed. A fog generator has been used to simulate obscurrants. In the past a rain and dust machine [12] were created to simulate more extreme operating conditions.

3.2 SICK LMS200 Laser Range Finder

The sensor we tested was the SICK LMS200. The LMS200 is a 2D scanning laser range finder. A beam of laser light is projected onto a rotating mirror. This mirror deflects the beam, creating a fan of laser light. Any object that breaks this fan reflects laser light back to the sensor. The distance is calculated based on how long the laser takes to bounce back to the sensor. The sensor is capable of performing scans at a rate of up to $75Hz$.

The LMS200 utilizes a class I eye-safe laser. The wave length of the laser is $905nm$. According to the manufacturer, the LMS200 has a range of $80m$ with an accuracy of $\pm 4cm$ and a 180° field of view with .5° resolution. This range is software selectable. The maximum detection distance can be shortened to increase the accuracy of measurements.

This sensor is very common among robotic ground vehicles, primarily because of its wide viewing angle and relatively long range. As the research done in [4] and [5] suggests, the detection range is well suited for rotorcraft operating in near-Earth environments. One major drawback to implementing this sensor on a rotorcraft is its size and weight. The LMS200 is $156 \times 155 \times 210mm$ and $4.5kg$, the majority of the weight coming from the ruggedized steel encasing.

From research in ground vehicles documented in [13] and [14], the SICK laser sensors are susceptible to airborne particulate matter such as dust. Using SISTR, we sought to quantify these effects.

3.3 Obscurant Characterization

One unique quality of SISTR is its ability to simulate weather conditions and other disturbances. With test rigs constructed inside the facility, sunlight, rain, fog and

other effects can be generated in a controlled, repeatable manner. Testing conditions and standards were determined using the US military guidelines for all weather performance outlined in [15]. All military vehicles are held to these standards, including UAVs.

Military standards acknowledge that smoke, fog and similar environmental factors can affect electro-optical systems. However, the standards fall short of defining requirements for these factors as these conditions are difficult to quantify. In this paper the amount of smoke is qualitatively asserted based on the "visibility" through the smoke. This is given as the distance that objects can be seen through the smoke.

The smoke was simulated using Superior Signal Company #3C smoke candles. These smoke candles issue 40,000 cubic feet of smoke over 3 minutes. The substance is actually a zinc-chloride mist, which is not the same content as naturally occurring smoke. However, as suggested in [1], particle size plays a major role in dispersing light. It is therefore assumed that the principle effect was still effectively modeled by this substance. This infrastructure provides a solid basis for determining the sensor model in the presence of obscurants.

To characterize the sensor, a sheet of white paper was placed 3m from the sensor aligned at 90° (in the middle of the sensing range). 500 data points were recorded and the resulting histogram plotted. Characterization was performed both with and without smoke.

For the smoke test, part of one of the smoke candles was used. Since the testing volume measured only 6,840 cubic feet, roughly 20% of the smoke candle material was extracted and ignited. After some dissipation, this produced smoke with a visibility of approximately 15m. The testing environment with and without smoke is shown in Fig. 5.

Fig. 5 To characterize the SICK LMS200, the sensor was placed inside the testing environment and pointed toward a white sheet of paper placed 3*m* away. 500 data points were recorded without smoke (*top*) and in smoke with a visibility of approx. 15*m* (*bottom*)

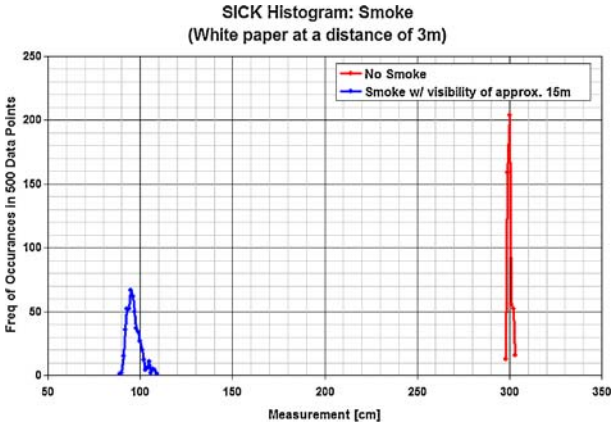

Fig. 6 Histogram of characterization tests performed with and without smoke. Without smoke the measurements are normally distributed around 300.05cm with a standard deviation of 1.11cm. When smoke is introduced, the distribution shifts far to the left and the deviation increases, showing that smoke blinds the sensor

The resulting histogram is shown in Fig. 6. Without smoke the sensor measurements are normally distributed about the correct distance of 3m. The mean of these measurements was 300.05cm with a standard deviation of 1.11cm. When smoke was introduced, the distribution shifted far to the left. Measurements in smoke had a mean of 96.5cm with a standard deviation of 3.63cm.

These results show that the LMS200 is blinded when the volume of its scanning area is filled with smoke. These results are consistent with qualitative assessments expressed from field tests of the sensor. The tests performed in the lab removed effects such as distribution from wind and rotor down wash, undeniably confirming that the sensor can not see through smoke. This information could now be used to interpret results of field testing the sensor.

4 Platform

Verification and validation of these test results was performed with a Rotomotion SR100 electric UAV helicopter, shown in Fig. 7. The SR100 is sold as a fully robotic helicopter capable of performing autonomous take off, landing, and GPS waypoint navigation when controlled from a laptop base station. Control from the base station to the helicopter is routed through an 802.11 wireless network adapter.

The SR100 has a rotor diameter of 2m allowing it to carry a payload of up to 8kg. For these experiments, we outfitted the helicopter with custom landing gear, a custom camera pan/tilt unit, the SICK LMS200, a serial to Ethernet converter, and two 12V batteries for payload power. In total we added approximately 7kg of payload. This greatly reduces the flight time, which is up to 45 min without a payload.

The biggest attraction of this platform, however, is the fact that it is already outfitted with all of the necessary sensors to calculate its pose. Gyros, an inertial measurement unit, and a magnetometer provide the craft's attitude and heading. This information is fused with a Novatel GPS system to provide position data. The position is reported as Cartesian coordinates relative to a global frame, who's origin is at the location where the helicopter was activated.

Fig. 7 The SR100 robotic helicopter from Rotomotion, Inc. The SR100 is sold as a fully robotic package capable of automated take off, landing, and GPS waypoint following

With the pose information already calculated, this platform enables mapping and landing zone identification using the algorithms described earlier.

5 Experimental Results

To determine the feasibility of performing mapping and safe landing zone identification in the presence of obscurants, verification and validation of the SISTR tests was performed. These tests were conducted at the research facility of Piasecki Aircraft. A

Fig. 8 The LMS200 was attached to the bottom of the SR100 helicopter and flown over smoke. Results showed that the LMS200 reflected off of the smoke, but was still able to locate flat terrain to land

location was found which contained a desirable landing area surrounded by cluttered terrain. The testing area used was a paved area surrounded by bushes and underbrush.

The helicopter was flown from a remote location, over the cluttered terrain, and into the desirable landing area. Simple software was written which evaluated the area directly beneath the helicopter to determine if it was flat. When the area was flat enough for the helicopter to land, the software displayed the scan as being green.

An initial test was conducted in the absence of smoke. During this test, the helicopter successfully identified the desirable landing area. Next, a smoke candle was placed in the desirable landing area and ignited. The test was repeated, this time with smoke obscuring the landing area. The results are depicted in Fig. 8.

As can be seen in the figure, the software successfully identified a flat region amongst the obscured area. However, the right side of the scan shows a detected obstacle depicted as a non flat region. Tests conducted in the lab confirmed that the sensor reflects off of smoke. It is therefore concluded that down wash exposed part of the obscured area, while the laser reflected off of the denser smoke.

6 Conclusions and Future Work

The results from the flight tests showed that the sensor detected a flat region amongst a smoke obscured area. Since previous tests inside a controlled environment proved that the sensor cannot see through smoke, it can be concluded that part of the obscured area was dispersed by down wash. This conclusion is further supported by video from the on board camera which suggests that there was smoke beneath the helicopter when a flat region was detected.

Now that the effect of smoke has been characterized and observed in the real world, we would like to incorporate these considerations into the algorithms outlined earlier. The mapping algorithm contains probabilistic models for both the pose sensors and the laser. The model of the sensor obtained from the characterization tests could be incorporated into this algorithm. If the helicopter is known to be flying over an obscured area, this model could be changed to match the conditions that the helicopter is operating in.

Furthermore, filters could be applied to the sensor data to remove noise from smoke or dust. This implementation could be augmented by providing the helicopter with existing terrain maps. In this scenario, laser scans gathered by the helicopter could be compared to the previously acquired terrain maps. The difference in information could be used to identify discrepancies in the two data sets. New obstacles that were introduced to the terrain such as cars and trucks would consistently appear in the helicopter scans. Noise from smoke or dust would appear inconsistent, and could then be filtered out.

However, the most plausible solution to this problem is to pair the LMS200 with a sensor that as capable of penetrating smoke. Previous work has shown us that sonar performs much better in the presence of airborne obscurants. If sonar is paired with the laser range finder, when the helicopter enters obscured conditions, more emphasis could be placed on the sonar data. We are currently in the process of investigating these avenues to create a sensor suite capable of navigating a helicopter in obscured conditions.

This paper showed how a cohesive design process of testing and evaluating followed by verification and validation can remove ambiguities in field testing robotic sensor suites. The lessons learned from these tests can be extended to many different sensor types and environmental effects. This framework provides a solid basis for developing UAV sensor suites and sensing algorithms, thereby decreasing developing time and reducing risks in field tests.

References

1. Dimmeler, A., Clement, D., Biichtemann, W.: Effects of obscurants on the performance of laser range finders. Technical Report 6, FGAN–FfO, Tubingen, Germany (1998)
2. Brinkworth, B.: Calculation of attenuation and back-scattering in cloud and fog. Atmos. Environ. **5**(8), 605–611 (1971)
3. Arshinov, Y.F., Donchenko, V.A., Zuev, V.E., Kostin1, V.V., Samokhvalov, I.V.: Experimental investigation of attenuation and backscatter of laser radiation at lambda=2.36 mu and lambda=0.63 mu by artificial fogs and smokes. Russ. Phys. J. **16**(6), 789–793 (1973)
4. Thrun, S., Diel, M., Hahnel, D.: Scan alignment and 3-d surface modeling with a helicopter platform. In: The 4th Int. Conf. on Field and Service Robotics, pp. 14–16 (2003)
5. Scherer, S., Singh, S., Chamberlain, L., Saripalli, S.: Flying fast and low among obstacles. In: International Conference on Robotics and Automation (ICRA), pp. 2023–2029 (2007)
6. Saripalli, S., Montgomery, J., Sukhatme, G.: Vision-based autonomous landing of an unmanned aerial vehicle. In: Int. Conf. on Robotics and Automation (ICRA), pp. 2799–2804 (2002)
7. Saripalli, S., Sukhatme, G.: Landing on a moving target using an autonomous helicopter. In: Int. Conf. on Field and Service Robotics (2003)
8. Johnson, A., Montgomery, J., Matthies, L.: Vision guided landing of an autonomous helicopter in hazardous terrain. In: Int. Conf. on Robotics and Automation, pp. 3966–3971 (2005)
9. Meingast, M., Geyer, C., Sastry, S.: Vision based terrain recovery for landing unmanned aerial vehicles. In: IEEE Conf. on Decision and Control (CDC), pp. 1670–1675 (2004)
10. Johnson, A., Klumpp, A., Collier, J., Wolf, A.: LIDAR-based hazard avoidance for safe landing on Mars. AIAA J. Guid. Control Dyn. **25**(6), 1091–1099 (2002)
11. Narli, V., Oh, P.: A hardware-in-the-loop test rig for designing near-earth aerial robotics. In: International Conference on Robotics and Automation (ICRA), pp. 2509–2514 (2006)
12. Sevcik, K.W., Oh, P.Y.: Designing aerial robot sensor suites to account for obscurants. In: International Conference on Intelligent Robots and Systems (IROS), pp. 1582–1587 (2007)
13. Thrun, S., Montemerlo, M., Dahlkamp, H., Stavens, D., Aron, A., Diebel, J., Fong, P., Gale, J., Halpenny, M., Hoffmann, G., Lau, K., Oakley, C., Palatucci, M., Pratt, V., Stang, P., Strohband, S., Dupont, C., Jendrossek, L.-E., Koelen, C., Markey, C., Rummel, C., van Niekerk, J., Jensen, E., Alessandrini, P., Bradski, G., Davies, B., Ettinger, S., Kaehler, A., Nefian, A., Mahoney, P.: Stanley, the robot that won the darpa grand challenge. Journal of Field Robotics **23**(9), 661–692 (2006)
14. Urmson, C., Ragusa, C., Ray, D., Anhalt, J., Bartz, D., Galatali, T., Gutierrez, A., Johnston, J., Harbaugh, S., Kato, H., Messner, W., Miller, N., Peterson, K., Smith, B., Snider, J., Spiker, S., Ziglar, J., Whittaker, W., Clark, M., Koon, P., Mosher, A., Struble, J.: A robust approach to high-speed navigation for unrehearsed desert terrain. Journal of Field Robotics **23**(8), 467–508 (2006)
15. Research, development, test and evaluation of materiel for extreme climatic conditions. Army Regulation, pp. 70–38 (1979)